A comparative study of multiple approaches to soil hydraulic parameter scaling applied at the hillslope scale

Raghavendra B. Jana[1] and Binayak P. Mohanty[1]

[1]   Soil hydraulic parameters were upscaled from a 30 m resolution to a 1 km resolution using four different aggregation schemes across the Little Washita watershed in Oklahoma. A topography-based aggregation scheme, a simple homogenization method, a Markov chain Monte Carlo (MCMC)-based stochastic technique, and a Bayesian neural network (BNN) approach to the upscaling problem were analyzed in this study. The equivalence of the upscaled parameters was tested by simulating water flow for the watershed pixels in HYDRUS-3-D, and comparing the resultant soil moisture states with data from the electronically scanned thin array radiometer (ESTAR) airborne sensor during the SGP97 hydrology experiment. The watershed was divided into pixels of 1 km resolution and the effective soil hydraulic parameters obtained for each pixel. The domains were then simulated using the physics-based HYDRUS-3-D platform. Simulated soil moisture states were compared across scales, and the coarse scale values compared against the ESTAR soil moisture data products during the SGP97 hydrology experiment period. Results show considerable correlations between simulated and observed soil moisture states across time, topographic variations, location, elevation, and land cover for techniques that incorporate topographic information in their routines. Results show that the inclusion of topography in the hydraulic parameter scaling algorithm accounts for much of the variability. The topography-based scaling algorithm, followed by the BNN technique, were able to capture much of the variation in soil hydraulic parameters required to generate equivalent soil moisture states in a coarsened domain. The homogenization and MCMC methods, which did not account for topographic variations, performed poorly in providing effective soil hydraulic parameters at the coarse scale.

1.   Introduction

[2]   Upscaling of soil hydraulic parameters is an issue of extreme importance in soil and water research. Water dynamics through the vadose zone is a major controlling factor in the hydrologic response of a watershed, and in the partitioning of incident precipitation into surface and subsurface components of the water balance in the basin. The vadose zone also acts as a filter against potential surface contaminants entering the groundwater. Modeling of related phenomena such as global circulation for climate prediction, river restoration, streamflow estimation, and fate and transport of contaminants, all require soil hydraulic parameter data from the vadose zone in some form or other. Some models directly utilize the soil hydraulic parameters such as the saturated hydraulic conductivity, the saturation water content, or the van Genuchten shape parameters as input data. Other models need the soil moisture state information, which can be simulated using the soil hydraulic parameters and the environmental conditions of the domain under study. All the above mentioned models have an inherent scale at which they are applied. For example, the climate prediction models work at very coarse, continental, or global scales. Streamflow models work at regional or watershed scales, while contaminant transport models work at fine, local scales. Soil moisture state may be measured at local scales using in situ sensors, or at coarse scales using satellite-based remote sensors. Soil hydraulic parameters, on the other hand, are generally measured at the local scales only. Measuring these parameters at all scales required by the above models is impractical both in economic, as well as in logistic sense. As a result, the need for efficient and accurate upscaling of fine scale soil hydraulic parameter data to coarser model scales is acutely felt by researchers.

[3]   A significant amount of variability exists in the vadose zone, both in terms of soil properties, as well as the geological and environmental factors. As coarser scales are considered, these variations increase [*Mohanty and Mousli*, 2000; *Vereecken et al.*, 2007]. At the finer local or field scales (meter scale), most variability is found in the soil texture and structure properties. At the hillslope (kilometer) scale, the variation in topography is added to the complexity. At

---

[1]Department of Biological and Agricultural Engineering, Texas A&M University, College Station, Texas 77843, USA.

yet larger watershed or regional (few hundred kilometers) scales, changes in vegetation are also significant. Upscaling is the process of replacing such a heterogeneous domain with effective homogeneous properties which generate the same responses such as soil moisture states, and surface and subsurface fluxes. Understanding how the hydraulic parameters are affected at different scales by the spatial variability of influencing factors such as soil structure and texture, vegetation, and topography is an inherent requirement of efficient scaling schemes. While it is known that connections exist between these factors and the hydraulic parameters [*Wu and Li*, 2006], the exact mathematical and/or physical nature of these connections is generally unknown. Over the past few decades, efforts to either understand these connections and solve these unknowns, or to find a way around them so as to obtain effective parameters at multiple scales have intensified.

[4] The Miller similitude theory [*Miller and Miller*, 1956; *Shouse and Mohanty*, 1998] took the first step toward this goal by reducing the dimensions of soil particles and pores in terms of a characteristic length scale. A detailed review of the history of upscaling methods developed over the years may be found in the work by *Vereecken et al.* [2007]. Most algorithms were developed to upscale soil hydraulic parameter data from local scales to slightly coarser field scales. As such, these methods are concerned with the variability in the soil texture and structure alone, and tend to ignore the effects of other factors such as topography or vegetation, on the parameter value. Since the coarser domain in these cases is of the order of a few hundred meters, this assumption of homogeneous terrain and vegetation may be reasonable. However, when applying these same scaling schemes at much larger extents, for example to satellite footprint scales of kilometers, this assumption is no longer valid. In an earlier study [*Jana and Mohanty*, 2012a] we developed an algorithm to explicitly account for changes in topography within a heterogeneous soil domain while upscaling soil hydraulic parameters to obtain effective values. The topography-based scaling algorithm was tested [*Jana and Mohanty*, 2012b] with field data across different topographic, vegetative, and pedological conditions in the Little Washita watershed, Oklahoma. Here we present a comparative study of the topography-based scaling scheme along with three other recent algorithms for soil hydraulic parameter upscaling. A simple homogenization technique, a Markov chain Monte Carlo approach, and a nonphysically based Bayesian neural networks approach to derive upscaled soil hydraulic parameters were compared with the topography-based scaling algorithm in this study.

2. Methods and Materials

2.1. Study Area

[5] The Little Washita (LW) River Watershed (Figure 1) in Oklahoma was selected as the test site for this study. Covering parts of Caddo, Comanche, and Grady counties of Oklahoma, the Little Washita River Watershed has an area of about 600 square kilometers, situated in the Southern Great Plains region of the United States. The Little Washita River is a tributary of the Washita River, which drains into the Red River on the Oklahoma-Texas border.

Hydrological and meteorological measurements of the watershed have been conducted for decades, providing scientists a long-term data source to study soil and water conservation, water quality, and basin hydrology [*Elliott et al.*, 1993]. Under continuous hydrological observation since 1936, the watershed has a network of sensors spread across its extent to measure rainfall, temperature, relative humidity, and soil radiation. In the 1990s, the United States Department of Agriculture's Agricultural Research Service (USDA-ARS) set up a network of 42 environmental monitoring stations called the ARS Micronet across this watershed. The watershed has also been the focus of several field experiments such as the Washita '92, Washita '94, Southern Great Plains 1997 (SGP97), Soil Moisture Experiments 2003 (SMEX03), and the Cloud and Land Surface Interaction Campaign (CLASIC) 2007.

[6] The LW region has a moderately rolling topography. The maximum elevation of the watershed is about 500 m above mean sea level, with a maximum relief of about 180 m. Rangeland and pastures are the dominant land use, with patches of winter wheat and other crops [*Allen and Naney*, 1991]. Soil textures range from fine sand to silty loam, with few exposed bedrock areas. The climate of the region is classified as subhumid/moist, with a mean annual precipitation of 760 mm and mean annual temperature of 16°C.

2.2. Data Sets

[7] Elevation data for the LW watershed at 30 m resolution was obtained from the National Elevation Data set from the USDA-NRCS Geospatial Data Gateway [http://datagateway.nrcs.usda.gov]. From the same source, the National Land Cover Data set, and the Soil Survey spatial and tabular data (SSURGO) were also obtained for the LW region. Daily precipitation and stream discharge data were obtained from the USDA-ARS Micronet database maintained by the Grazinglands Research Laboratory [http://ars.mesonet.org/] for the months of April–July 1997. Precipitation data from the 42 meteorological observation stations across the watershed were used to create daily precipitation maps by kriging. The corresponding precipitation value for each pixel was assigned as the time dependent boundary condition for the day.

[8] Soil moisture data products from the electronically scanned thin array radiometer (ESTAR) for the LW region are available from the NASA-GSFC's Goddard Earth Sciences Data and Information Services Center [http://daac.gsfc.nasa.gov/]. The ESTAR data is collected using the L-band passive microwave mapping instrument mounted on an airplane. The sensor measures the microwave brightness temperatures, which are then converted to predict soil moisture estimates. The data are processed to produce geo-referenced gridded products for each day of observation at a pixel resolution of 800 m. A detailed description of the ESTAR data and processing may be found in the work by *Jackson et al.* [1999]. The ESTAR soil moisture data product was used in this study to validate the outputs from the simulation of the LW domain using HYDRUS-3-D. ESTAR soil moisture data is available for 16 days in the period between mid-June and mid-July 1997 (DOY 169 to 197). This is the period during which the SGP97 hydrology experiment was conducted in the LW region [*Mohanty et al.*, 2002].
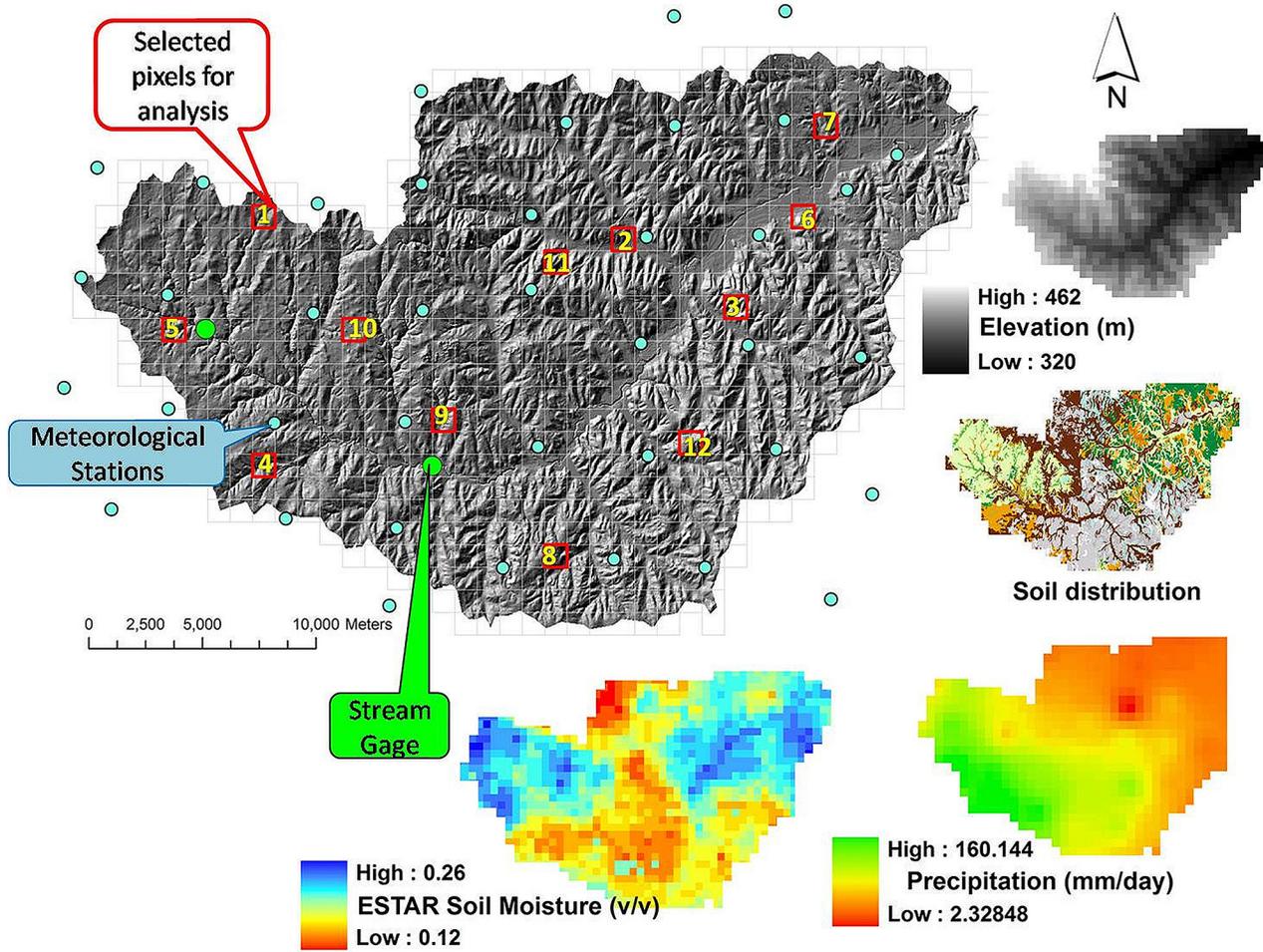
Figure 1. Little Washita watershed study area, location of selected pixels, stream gauges, meteorological stations, and some input layers for modeling.

2.3. Physical Domain Setup

[9] The HYDRUS-3-D hydrologic simulation software [*Šimůnek et al.*, 2006] was used to simulate the soil domains. The HYDRUS software package solves the modified Richards' equation for water flow in saturated/unsaturated domains using numerical techniques. The HYDRUS software allows the user to analyze water flow through saturated, partially saturated or unsaturated regions with irregular boundaries, and composed of nonuniform soils. HYDRUS-3-D allows for three dimensional flow representations in the unsaturated zone. The governing flow equation, a modified form of the Richard's equation, is given by

$$\frac{\partial \theta}{\partial t} = \frac{\partial}{\partial x_i}\left[K\left(K_{ij}^A \frac{\partial h}{\partial x_j} + K_{iz}^A \right) \right] - S, \qquad (1)$$

where θ is the volumetric water content, h is the pressure head, S is a sink term, $x_i(i = 1, 2)$ are the spatial coordinates, t is time, K_{ij}^A are components of a dimensionless anisotropy tensor K^A, and K is the unsaturated hydraulic conductivity, given by

$$K(h, x, y, z) = K_s(x, y, z) K_r(h, x, y, z), \qquad (2)$$

where K_r and K_s are the relative and saturated hydraulic conductivities.

[10] The entire Little Washita watershed was divided into a grid of 1000 m $\times$ 1000 m pixels (Figure 1). Twelve pixels of 1 km $\times$ 1 km size were selected from across the watershed for analysis, based on their location, topography, land cover, and soil type so as to encompass the variety in the watershed, as shown in Figure 1. Elevation data at 30 m resolution was extracted for each selected pixel using a GIS software. The data was then fed to the HYDRUS-3-D environment to create the geometry of the domain. A minimum soil depth of 6 m was maintained across all pixels. Corresponding soil properties data from the SSURGO database are extracted for each pixel and, using the ROSETTA [*Schaap et al.*, 2001] framework within HYDRUS-3-D, the corresponding soil hydraulic parameters for the van Genuchten-Mualem model with no hysteresis were obtained. The Mualem-van Genuchten functions [*van Genuchten*, 1980] are

$$S_e = \frac{\theta(h) - \theta_r}{\theta_s - \theta_r} = \left[\frac{1}{1 + |\alpha h|^n} \right]^m, \qquad (3)$$

$$K(h) = K_s S_e^{\lambda}[1 - (1 - S_e^{1/m})^m]^2, \qquad (4)$$

where water content θ is a nonlinear function of pressure head h, S_e is the relative saturation (–), θ_r and θ_s are the residual and saturated water contents ($cm^3\ cm^{-3}$), respectively, α (cm^{-1}), n (–), m (–), and λ (–) are shape parameters of the retention and the conductivity functions, K_s is the saturated hydraulic conductivity ($cm\ d^{-1}$), and $m = 1-1/n$.

[11] These soil types were designated in the HYDRUS-3-D domain. Similarly, for each pixel domain, the land cover data is extracted and suitable root water uptake parameters are assigned. The Feddes model for the root water uptake was applied in our study, with a maximum rooting depth of 1 m, and no solute stress. Water tables were assigned to the domain based on its location in the watershed following the study by *Kollet and Maxwell* [2008]. Pixels close to the streambed had water tables at 1 m, while those farthest from the stream were assigned water tables at 4 m depths.

[12] Finite element meshes were generated for each pixel with 20 horizontal layers and node spacing of 30 m. The top surface was assigned an "atmospheric boundary" condition, while the walls of soil plot were designated as seepage faces to enable lateral flow of water through the soil domain. The lower boundary had a deep drainage condition. The mathematical formulations and features of the boundary conditions are given by *Jana and Mohanty* [2012a]. Initial condition of the soil profile was given by soil water content just under saturation for the domain since a significant precipitation even occurred immediately before the commencement of the simulations.

[13] Initially, each node in the FEM was assigned one of the soil types based on the fine scale SSURGO data. The five soil hydraulic parameters—residual soil water content (θ_r); saturation water content (θ_s); van Genuchten parameters α and N; and the saturated hydraulic conductivity K_s were upscaled using each of the methods described below to the coarse (1 km) resolution. Instead of coarsening the FEM grid, we assigned the aggregated effective soil hydraulic parameters to each node within the upscaled pixel footprint. This was done so that the computational integrity of the FEM is consistent across all scales. It must be noted that while the soil types or hydraulic parameter values are assigned by the user to the nodes, the HYDRUS program interpolates the values to the 3-D elements in the mesh. The pixel domains with the upscaled soil hydraulic parameters are then put through the same simulation and soil moisture updating procedure as before.

[14] Each 1000 m × 1000 m pixel is simulated in HYDRUS individually for a period of 1 day at a time. Using the elevation information at 1 km, the flow direction of surface water out of each pixel is determined using a *d-inf* algorithm as described by *Tarboton* [1997]. Surface runoff generated daily by each pixel is computed as the difference between the precipitation and the infiltration. This excess water is then routed to the downstream pixel based on the flow direction map, and the surface soil moisture of the downstream pixel updated to reflect the increased water content. Subsurface flux connections between individual pixels were implemented using seepage faces. Seepage face boundary conditions allow for the removal of water from the saturated portions of the domain boundary. This volume of water ejected from each cross sectional boundary above the water table is added to the nodes of the adjacent pixel's seepage face which are above the water table

and have not attained saturation, at each daily time step to update the soil water contents in the subsurface layers.

[15] Once all pixels have been updated, they are then simulated for the next day. This process is repeated for the duration of simulation period which spanned for three months—from mid-April 1997 to mid-July 1997. The first two months were considered as the model spin-up time to allow the domain characteristics to stabilize, and only outputs for the last 1 month were used in the analysis.

2.4. Topography-Based Aggregation

[16] The power average operator, as described by *Yager* [2001] is used in this study to coarsen the soil hydraulic parameter values, as implemented by *Jana and Mohanty* [2012a, 2012b]. Two types of aggregating methods are combined in this technique. In mode-like methods, the emphasis is on finding the most probable value of a parameter from a given set [*Yager*, 1996]. In mean type aggregation, the goal is to find the average value of the given set. By combining the features of both the aggregating methods, the power average technique provides itself as an ideal tool for use in scaling of soil hydraulic parameters. Generally, soil pedons clustered around a location tend to have similar properties, with the correlation dying out as the distance between two points increases. This means that the aggregating method must take into consideration the mutual support the pedons extend to each other when clustered.

[17] The power average operator is defined as

$$P^*(p_1, p_2, \ldots, p_n) = \frac{\sum_{i=1}^{n}[1 + T(p_i)]p_i}{\sum_{i=1}^{n}[1 + T(p_i)]}, \quad (5)$$

where

$$T(p_i) = \sum_{\substack{j=1 \\ j \neq i}}^{n} Sup(p_i, p_j), \quad (6)$$

P^* is the power average of the parameter values $p_1 \ldots p_n$. $Sup(p_i, p_j)$ is the support for p_i from p_j. This feature allows data clustered around a particular value to combine nonlinearly while being aggregated. The support function is the crux of the power average method. A general form of the support equation is given by

$$Sup(p_i, p_j) = e^{-\eta(p_i - p_j)^z}, \quad (7)$$

where $\eta \geq 0$. This function is continuous, symmetric and lies in the unit interval, as required. The power law form of the support function is similar to the form of the transmissivity profile used in the TOPMODEL algorithm to compute the topographic index [*Iorgulescu and Musy*, 1997].

[18] The model parameter η can be considered as a scale parameter. Since other factors such as vegetation and environmental variations are held constant in this case, η depends on the elevation differential and the distance between observations. The value of η is given by the formula

$$\eta = \left(\frac{z_{j_{max}} - z_{j_{min}}}{z_i - z_j}\right)^2 * \frac{\sqrt[2]{(x_i - x_j)^2 + (y_i - y_j)^2 + (z_i - z_j)^2}}{S}. \quad (8)$$

Here x, y, and z are the Cartesian coordinates of the point, while S is the scale (resolution) to which the hydraulic parameters are being aggregated. The first term on the right-hand side is the normalized difference in elevation between the two locations i and j. The second term provides the linear distance between measurement values, normalized by the scale dimension. A distance which may be considered as "far" at one scale may not be so at a coarser scale. Hence, normalizing the actual distance by the scale dimension provides a more meaningful way of computing the support function.

2.5. Homogenization

[19] Homogenization of soil hydraulic parameters is a simple way of upscaling by spatially averaging the soil hydraulic parameters. *Zhu and Mohanty* [2002] examined the impact of areal heterogeneity of soil hydraulic parameters on the ensemble response of a pixel-size domain. Different parameter averaging schemes were considered and their outputs compared with effective parameters computed in the basis of the ensemble flux dynamics. Arithmetic, geometric, and harmonic averages of the van Genuchten parameters a and n were tested along with arithmetic mean for K_s. Based on their study, they suggested that for averaging spatial variability, arithmetic means could be used for the K_s and n parameters, while the upscaled α parameter would have a value between the harmonic and arithmetic means, based on the correlation of α with K_s. In this comparative study we computed the arithmetic, geometric, and harmonic averages for the soil hydraulic parameters in the 12 selected pixels in the LW watershed.

2.6. Markov Chain Monte Carlo-Based Upscaling

[20] A Markov chain Monte Carlo (MCMC) based upscaling algorithm developed by *Das et al.* [2008] to evaluate satellite based soil moisture measurements was adapted for this comparative study. The original work focused on the soil moisture data product from the advanced microwave scanning radiometer (AMSR-E) located on NASA's Aqua satellite. The approach of *Das et al.* [2008] was to derive the upscaled effective soil hydraulic parameters from a time series of soil moisture data at the AMSR-E footprint scale, and stochastic information of the fine scale soil hydraulic parameter variability. The upscaling algorithm was developed within a Bayesian framework to produce probability distributions of the parameters. In place of the AMSR-E soil moisture product, we used the ESTAR soil moisture obtained using airborne sensors, as described above. This was done in order to compare the performance of the algorithm at the hillslope scales where the ESTAR measurements are representative, rather than at the much coarser AMSR-E footprint scale.

[21] In a Bayesian framework, pre-existing knowledge about the parameters of a model can be combined with actual observations and model outputs. The resulting probability distribution of the parameter, also called the posterior distribution, provides an estimate of the uncertainty in the parameter value based on the prior knowledge and the sampled data values. Model parameters are considered as random variables, each with a particular probability density function (pdf) [*Gelman et al.*, 1995]. Soil hydraulic parameters of the dominant soil type within a footprint based on Soil Survey

Geographic (SSURGO) database were assigned as priors. The Mualem-van Genuchten functions (equations (3) and (4)) were used in this study. A normal distribution was assigned to all the hydraulic parameters based on the SSURGO database.

[22] *Das et al.* [2008] introduce a scale parameter β, with a noninformative, uniform prior, to account for the scale disparity. β relates fine scale parameters to the effective coarse scale parameter in the form

$$(P)_{\text{effective}} = P^{\beta}, \tag{9}$$

where P is any soil hydraulic parameter. A set of upscaled parameters was obtained such that

$$z_i = (\theta_r^{\beta i}, \theta_s^{\beta i}, \alpha^{\beta i}, n^{\beta i}, K_s^{\beta i})_i, \tag{10}$$

where i is an MCMC realization and βi is the corresponding scale parameter.

[23] By Bayes theorem, the condition posterior probability is given by

$$P(Z|D) = \frac{P(Z)P(D|Z)}{P(D)}. \tag{11}$$

Here D is the set of measured soil moisture values and $P(Z)$ is the prior joint pdf for the upscaled parameters. $P(D)$ is a normalizing factor while $P(D|Z)$ is the likelihood derived from the coarse scale soil moisture measurements. A detailed description the of algorithm to obtain the posterior pdfs of each of the parameters using a Metropolis algorithm can be found in the paper by *Das et al.* [2008] and are not repeated here. As mentioned, suitable changes were made to the algorithm to incorporate ESTAR measurements in place of the AMSR-E soil moisture product, without compromising on the integrity of the algorithm.

2.7. Multiscale Bayesian Neural Networks

[24] The last upscaling model to be compared was developed by *Jana et al.* [2008] as a means of applying an artificial neural networks-based pedotransfer function across scales, within a Bayesian framework. The technique consists of training a Bayesian neural network (BNN) with soil texture and structure data at one scale, and to simulate the soil water retention at another. *Jana et al.* [2008] and *Jana and Mohanty* [2011] applied the multiscale BNN to downscale soil properties from the SSURGO (30 m) resolution to the point scale. Training inputs to the BNN consist of the percentage of sand, silt, and clay, and the bulk density of the soil, and elevation and vegetation data. The targets were the soil water contents at 0, 0.33, and 15 bars.

[25] If y is the target and x the input data, then the relation between x and y can be described as

$$y = f(x|w) + E, \tag{12}$$

where $f(x|w)$ is the functional approximation (described by the ANN) of the relationship between the input and the target, w is the vector of weights and biases for the layers of ANN neurons, and E is the error term. Conventional (standard/deterministic) ANN methodology attempts to find a single set of weights w such that given the training

inputs x the network reproduces the training targets y with minimal error E. Bayesian ANNs, however, generate a probability distribution of the layer weights which is dependent on the given input data. Using MCMC techniques, the BNN provides a distribution of the output parameter instead of a single deterministic value.

[26] In this study, we adapted the BNN for upscaling the soil water content. Training data were still obtained from the SSURGO database and the 30 m resolution DEM. The simulation data (soil texture and structure) were obtained from the coarser resolution (1 km) STATSGO database and the 1 km Dem, as mentioned in section 2.2. Since neither the SSURGO or the STATSGO databases report values for the van Genuchten parameters α and n, these were estimated from the ROSETTA database within HYDRUS-3-D for both scales. The soil texture and structure data from STATSGO, and the simulated soil water contents at 0.33 and 15 bars form the inputs to ROSETTA at the coarse scale. Neural networks with one input layer, one hidden layer with five neurons, and one output layer were used, with the tangent hyperbolic transfer function, for all cases. This architecture was decided based on the studies by *Jana and Mohanty* [2008].

3. Results and Discussion

[27] Five soil hydraulic parameters—θ_r, θ_s, α, n, and K_s—were upscaled using the four different upscaling methodologies from 30 m resolution to 1 km resolution for the 12 selected pixels of 1 km $\times$ 1 km size within the LW watershed. Table 1 shows the average elevation (at 1 km resolution), land cover, and average compound topographic index values for the 12 selected pixels. Table 2 shows the fine scale soil hydraulic properties of the materials in the 12 pixels. Except for pixel 4, all other pixels had at least three different soil types distributed in the pixel. The effective soil hydraulic parameter values from each upscaling scheme were compared with the values from the topography-based upscaling. Average daily surface soil moisture states were compared for these pixels for the 16 days on which the ESTAR data product is available.

3.1. Comparison of Upscaled Soil Hydraulic Parameters

[28] Aggregate values for the five soil hydraulic parameters at the 1 km scale, as obtained from the four different

Table 1. Elevation, Land Cover and Topographic Index Details of 12 Selected Pixels in Little Washita Watershed[a]

	Average Elevation (m)	Land Cover	Average CTI
Pixel 1	446	Pasture	7.332
Pixel 2	355	Pasture	7.312
Pixel 3	369	Pasture	6.656
Pixel 4	408	Bare	6.846
Pixel 5	410	Bare	6.846
Pixel 6	345	Wheat	7.379
Pixel 7	341	Wheat	7.396
Pixel 8	407	Bare	7.128
Pixel 9	392	Pasture	6.709
Pixel 10	419	Wheat	7.274
Pixel 11	377	Pasture	7.085
Pixel 12	394	Pasture	7.247

[a]Values are reported at the 1 km resolution.

Table 2. Soil Hydraulic Parameter Data at Fine (30 m) Scale for the 12 Selected Pixels

	Material	θ_r (m^3 m^{-3})	θ_s (m^3 m^{-3})	α (m^{-1})	n (–)	K_s (m d^{-1})
Pixel 1	1	0.04	0.38	1.3000	1.3420	0.6773
	2	0.04	0.37	1.1400	1.3285	0.2202
	3	0.04	0.36	0.8300	1.4252	0.2202
	4	0.05	0.40	0.9700	1.3810	0.2202
Pixel 2	1	0.04	0.38	1.3000	1.3420	0.5587
	2	0.04	0.37	0.8100	1.4307	0.2202
	3	0.05	0.38	1.2200	1.3602	0.6773
	4	0.04	0.36	0.8300	1.4252	0.2202
	5	0.05	0.39	0.9000	1.3892	0.2202
Pixel 3	1	0.05	0.38	1.2200	1.3602	0.5300
	2	0.04	0.36	0.8300	1.4252	0.2400
	3	0.05	0.41	1.0100	1.3722	0.2158
Pixel 4	1	0.04	0.36	1.5600	1.3498	0.2822
	2	0.05	0.39	1.2100	1.3597	0.0917
Pixel 5	1	0.04	0.37	0.8400	1.4362	0.2562
	2	0.05	0.39	1.0200	1.3716	0.1133
	3	0.05	0.40	0.9700	1.3810	0.2145
	4	0.07	0.44	1.4800	1.3003	0.1256
Pixel 6	1	0.04	0.37	0.8100	1.4307	0.1655
	2	0.05	0.38	1.2200	1.3602	0.1549
	3	0.05	0.40	0.9400	1.3770	0.1982
Pixel 7	1	0.04	0.36	1.6300	1.3442	0.3298
	2	0.05	0.39	0.8800	1.3739	0.0890
	3	0.05	0.38	1.2200	1.3602	0.1549
	4	0.05	0.39	0.9000	1.3892	0.1993
Pixel 8	1	0.03	0.36	2.0400	1.4414	1.6038
	2	0.02	0.36	1.5600	1.3636	0.7068
	3	0.03	0.38	2.0400	1.3662	0.9750
	4	0.04	0.38	1.3000	1.3420	0.4257
Pixel 9	1	0.02	0.36	1.5600	1.3636	0.7068
	2	0.04	0.38	1.3000	1.3420	0.4257
	3	0.04	0.37	1.2900	1.3466	0.4270
Pixel 10	1	0.05	0.39	1.0200	1.3716	0.1133
	2	0.07	0.44	1.4800	1.3003	0.1256
	3	0.04	0.37	0.8400	1.4362	0.2562
	4	0.05	0.40	0.9700	1.3810	0.2145
Pixel 11	1	0.05	0.39	2.3400	1.3306	0.3568
	2	0.05	0.38	1.2200	1.3602	0.1549
	3	0.04	0.36	0.8300	1.4252	0.2401
Pixel 12	1	0.02	0.36	1.5600	1.3636	0.7068
	2	0.03	0.38	2.0400	1.3662	0.9750
	3	0.04	0.36	1.5700	1.3424	0.3238

upscaling algorithms are reported in Table 3. Since the MCMC and BNN methodologies provide a distribution for each parameter, the maximum, minimum, and average values are reported for these methods. Upscaled values of the five soil hydraulic parameters, as obtained from the homogenization methods for each pixel are plotted in Figure 2, along with those obtained from the topography-based scaling scheme. As can be seen from Table 3, and in Figure 2, the arithmetic, geometric, and harmonic averages for each parameter are very close to each other. Only in the values for the van Genuchten α and K_s, slight deviations are observed. Table 4 provides correlation information between the homogenized soil hydraulic parameters and those obtained from the topography-based scaling scheme. It can be seen that the best correlations were obtained for the soil water contents θ_r and θ_s, while the van Genuchten n parameter was the least correlated. It is seen in Figure 2 that in most cases the n parameter is overpredicted by homogenization as compared with the topography-based scaling output. The parameter n is dependent on the particle size distribution of the soil, which in turn may be dictated by the topography of the

Table 3. Soil Hydraulic Parameters at the Coarse (1 km) Scale for the 12 Selected Pixel in the Little Washita Region, As Obtained From the Different Upscaling Algorithms[a]

Upscaling Method		θ_r (m^3 m^{-3})	θ_s (m^3 m^{-3})	α (m^{-1})	n (–)	K_s (m d^{-1})
Pixel 1						
Topo-based		0.04	38	1.236	1.349	0.587
Homogenization	Arithmetic	0.04	38	1.060	1.369	0.334
	Geometric	0.04	38	1.045	1.369	0.292
	Harmonic	0.04	38	1.030	1.368	0.265
MCMC	Max	0.09	38	1.036	1.828	
	Min	0.03	12	0.451	1.352	
	Average	0.06	30	0.820	1.582	0.797
BNN	Max	0.04	42	2.381	1.549	0.293
	Min	0.03	31	1.739	1.131	0.214
	Average	0.03	36	2.070	1.347	0.255
Pixel 2						
Topo-based		0.04	38	1.149	1.368	0.483
Homogenization	Arithmetic	0.04	38	1.012	1.389	0.379
	Geometric	0.04	38	0.992	1.389	0.332
	Harmonic	0.04	38	0.973	1.389	0.296
MCMC	Max	0.13	40	1.044	2.425	
	Min	0.04	8	0.396	1.553	
	Average	0.09	28	0.710	2.115	0.473
BNN	Max	0.06	44	1.334	1.562	0.176
	Min	0.04	0.32	0.974	1.141	0.128
	Average	0.05	0.39	1.160	1.359	0.153
Pixel 3						
Topo-based		0.05	0.38	1.159	1.367	0.464
Homogenization	Arithmetic	0.05	0.38	1.020	1.386	0.329
	Geometric	0.05	0.38	1.008	1.386	0.302
	Harmonic	0.05	0.38	0.995	1.385	0.281
MCMC	Max	0.13	0.38	1.048	1.860	
	Min	0.03	0.11	0.560	1.389	
	Average	0.09	0.25	0.900	1.642	0.344
BNN	Max	0.06	0.44	1.334	1.562	0.176
	Min	0.04	0.32	0.974	1.141	0.128
	Average	0.05	0.39	1.160	1.359	0.153
Pixel 4						
Topo-based		0.04	0.38	1.306	1.357	0.144
Homogenization	Arithmetic	0.04	0.37	1.385	1.355	0.187
	Geometric	0.04	0.37	1.374	1.355	0.161
	Harmonic	0.04	0.37	1.363	1.355	0.138
MCMC	Max	0.12	0.41	1.034	1.816	
	Min	0.03	0.10	0.461	1.266	
	Average	0.07	0.23	0.836	1.551	0.434
BNN	Max	0.03	0.41	2.519	1.555	0.346
	Min	0.03	0.30	1.840	1.136	0.253
	Average	0.03	0.35	2.190	1.352	0.301
Pixel 5						
Topo-based		0.06	0.42	1.247	1.339	0.166
Homogenization	Arithmetic	0.05	0.40	1.078	1.372	0.177
	Geometric	0.05	0.40	1.053	1.371	0.167
	Harmonic	0.05	0.40	1.032	1.371	0.158
MCMC	Max	0.12	0.38	1.037	1.801	
	Min	0.04	0.11	0.416	1.381	
	Average	0.09	0.27	0.730	1.558	0.036
BNN	Max	0.07	0.48	1.472	1.511	0.241
	Min	0.05	0.35	1.075	1.104	0.176
	Average	0.06	0.42	1.280	1.314	0.210
Pixel 6						
Topo-based		0.04	0.38	0.939	1.404	0.167
Homogenization	Arithmetic	0.05	0.38	0.976	1.389	0.172
	Geometric	0.04	0.38	0.962	1.389	0.171
	Harmonic	0.05	0.38	0.990	1.389	0.173
MCMC	Max	0.12	0.36	1.031	2.333	
	Min	0.03	0.09	0.373	1.566	
	Average	0.09	0.27	0.814	2.123	0.627
BNN	Max	0.04	0.42	1.449	1.594	0.177
	Min	0.03	0.31	1.058	1.164	0.129
	Average	0.04	0.37	1.260	1.386	0.154

Table 3. (continued)

Upscaling Method		θ_r (m^3 m^{-3})	θ_s (m^3 m^{-3})	α (m^{-1})	n (–)	K_s (m d^{-1})
		Pixel 7				
Topo-based		0.05	0.37	1.321	1.357	0.232
Homogenization	Arithmetic	0.05	0.38	1.158	1.367	0.193
	Geometric	0.05	0.38	1.120	1.367	0.174
	Harmonic	0.05	0.38	1.087	1.367	0.155
MCMC	Max	0.12	0.37	1.057	2.218	
	Min	0.04	0.11	0.507	1.629	
	Average	0.09	0.23	0.846	1.947	0.062
BNN	Max	0.04	0.42	1.449	1.594	0.177
	Min	0.03	0.31	1.058	1.164	0.129
	Average	0.04	0.37	1.260	1.386	0.154
		Pixel 8				
Topo-based		0.02	0.36	1.560	1.364	0.707
Homogenization	Arithmetic	0.03	0.37	1.735	1.378	0.928
	Geometric	0.03	0.37	1.704	1.378	0.828
	Harmonic	0.03	0.37	1.673	1.377	0.739
MCMC	Max	0.11	0.37	1.036	1.781	
	Min	0.03	0.06	0.353	1.256	
	Average	0.06	0.23	0.688	1.517	0.547
BNN	Max	0.04	0.42	5.003	1.590	0.760
	Min	0.03	0.30	3.654	1.161	0.555
	Average	0.03	0.36	4.350	1.382	0.661
		Pixel 9				
Topo-based		0.03	0.37	1.408	1.352	0.544
Homogenization	Arithmetic	0.03	0.37	1.383	1.351	0.520
	Geometric	0.03	0.37	1.378	1.351	0.505
	Harmonic	0.03	0.37	1.373	1.351	0.491
MCMC	Max	0.12	0.39	1.041	1.765	
	Min	0.03	0.07	0.411	1.306	
	Average	0.08	0.28	0.875	1.541	0.494
BNN	Max	0.04	0.42	5.003	1.590	0.760
	Min	0.03	0.30	3.654	1.161	0.555
	Average	0.03	0.36	4.350	1.382	0.661
		Pixel 10				
Topo-based		0.05	0.40	0.993	1.383	0.213
Homogenization	Arithmetic	0.05	0.40	1.078	1.372	0.177
	Geometric	0.05	0.40	1.053	1.371	0.167
	Harmonic	0.05	0.40	1.032	1.371	0.158
MCMC	Max	0.13	0.38	1.039	1.694	
	Min	0.03	0.08	0.407	1.276	
	Average	0.08	0.28	0.870	1.479	0.573
BNN	Max	0.08	0.47	2.105	1.440	0.198
	Min	0.06	0.34	1.537	1.052	0.145
	Average	0.07	0.41	1.830	1.252	0.172
		Pixel 11				
Topo-based		0.04	0.38	1.591	1.372	0.282
Homogenization	Arithmetic	0.04	0.38	1.463	1.372	0.251
	Geometric	0.04	0.38	1.333	1.371	0.237
	Harmonic	0.04	0.38	1.224	1.371	0.223
MCMC	Max	0.12	0.38	0.964	1.803	
	Min	0.03	0.07	0.312	1.243	
	Average	0.08	0.22	0.618	1.497	0.052
BNN	Max	0.06	0.44	1.334	1.562	0.176
	Min	0.04	0.32	0.974	1.141	0.128
	Average	0.05	0.39	1.160	1.359	0.153
		Pixel 12				
Topo-based		0.03	0.36	1.633	1.359	0.648
Homogenization	Arithmetic	0.03	0.37	1.723	1.357	0.669
	Geometric	0.03	0.37	1.710	1.357	0.607
	Harmonic	0.03	0.37	1.697	1.357	0.543
MCMC	Max	0.12	0.39	1.051	2.413	
	Min	0.03	0.07	0.309	1.386	
	Average	0.07	0.26	0.691	2.031	0.298
BNN	Max	0.04	0.42	5.003	1.590	0.760
	Min	0.03	0.30	3.654	1.161	0.555
	Average	0.03	0.36	4.350	1.382	0.661

[a]Topo-based: topography-based scaling scheme; MCMC: Markov chain Monte Carlo-based scaling scheme; BNN: Bayesian neural networks-based scaling scheme.
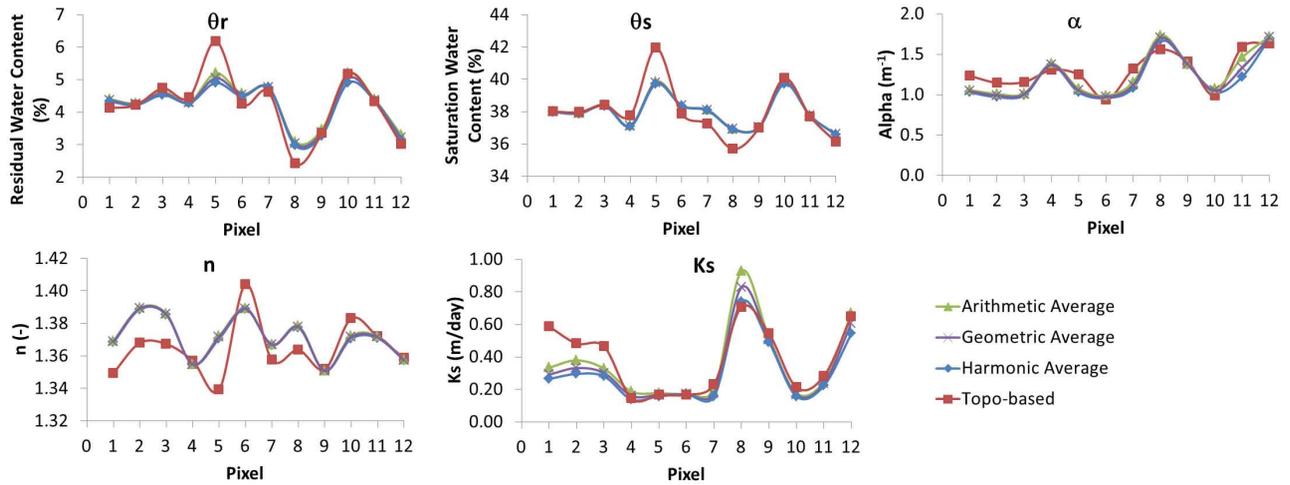
Figure 2. Plots of upscaled soil hydraulic parameters obtained by homogenization and topography-based upscaling techniques.

location. A simple homogenization may not be able to capture the clustering of n values based on the relative elevations within a domain; a factor which is considered in the topography-based scaling. This could be the reason for the low correlation of the parameter. Keeping in line with the guidelines suggested by *Zhu and Mohanty* [2002], the arithmetic average values of all parameters but the van Genuchten α were used in the simulation using HYDRUS-3-D. For α, the geometric average, which lies between the arithmetic and harmonic averages, was used.

[29] Upscaled hydraulic parameter values obtained from the MCMC-based algorithm are plotted in Figure 3, along with the parameters from the topography-based scheme. As mentioned before, the MCMC algorithm, as implemented by *Das et al.* [2008] provides a distribution for each parameter, but for K_s. While the water content values θ_r and θ_s mostly fall within the range of possible values from the MCMC iterations, the shape parameters, α and n, rarely do so. The correlations between the averages of the MCMC derived parameters and the topography based scaling outputs are also reported in Table 4. It is seen that the correlations are quite low for most parameters. MCMC is a statistical technique, rather than a physical model. In the form as implemented by *Das et al.* [2008] and adapted here, it solves the van Genuchten equations (equations (3)

and (4)) at a particular pressure such that the soil moisture value $\theta(h)$ is obtained. This value is compared with the provided ESTAR value and accepted with a particular probability. With a combination of five parameters working to match a single value, the matter of nonuniqueness enters. A total of 45,000 MCMC samples were retained for each parameter, after discarding an initial 5000 samples as model burn-in, with an acceptance rate of around 12%. It is possible that having a larger set of retained samples could widen the range of probable values. For simulation of the soil domain in HYDRUS-3-D, the average values from the MCMC outputs were used for all soil hydraulic parameters.

[30] Variations across the 12 selected pixels in the upscaled soil hydraulic parameters estimated by the BNN methodology are plotted in Figure 4. From the plots, it is apparent that the θ_s parameter is the best correlated, and is verified from Table 4. It should be remembered here that the shape parameters of the van Genuchten equation a and n were not upscaled using the BNN methodology, but were derived from the ROSETTA database from the coarse resolution soil texture and structure properties, and the upscaled soil water contents at 0.33 and 15 bars.

3.2. Comparison of Average Soil Moisture State With ESTAR Measurements

[31] The 2 selected pixels of the Little Washita watershed were simulated for water movement using HYDRUS-3-D for the three month period beginning mid-April 1997. The first two months were used as model spin-up time to allow for the soil domain characteristics to settle. Analysis is made of only the last month beginning mid-June (DOY 169 to 197). This is the period when the SGP97 experiment was conducted, and hence the availability of the ESTAR data for this period.

[32] Figure 5 shows the average daily surface soil moisture for each pixel simulated using the different sets of soil hydraulic parameters from the four upscaling methods compared here, along with the ESTAR measurements. It is seen that in most cases, the MCMC-predicted parameters cause an overprediction of the soil moisture state. The

Table 4. Pearson's Correlations for Each Soil Hydraulic Parameter Obtained From Each Upscaling Algorithm With Those Obtained From the Topography-Based Upscaling Scheme, Across All Pixels

Average	θ_r	θ_s	α	n	K_s
Arithmetic	0.95[a]	0.91[a]	0.89[a]	0.56[b]	0.88[a]
Geometric	0.94[a]	0.91[a]	0.85[a]	0.56[b]	0.87[a]
Harmonic	0.92[a]	0.91[a]	0.82[a]	0.56[b]	0.87[a]
MCMC	0.72[a]	0.32	−0.60[b]	0.36	0.36
BNN	0.68[b]	0.85[a]	0.61[b]	−0.03	0.69[b]

[a]Correlations significant at the 0.01 level.
[b]Correlations significant at the 0.05 level.
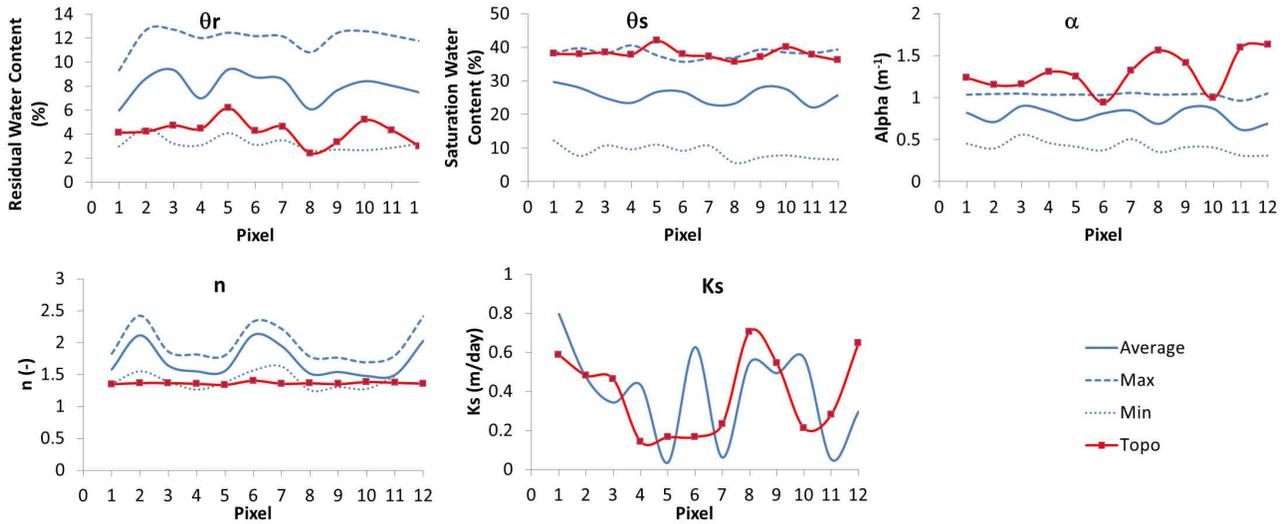
Figure 3. Plots of upscaled soil hydraulic parameters obtained by MCMC-based and topography-based upscaling techniques.

homogenized parameters too tend to overpredict the soil moisture in certain cases, especially during the wetter days. It is also seen that the topography-based and BNN soil moisture signatures closely follow each other for the most part. Correlations of the average daily soil moisture simulated using the homogenization, MCMC and BNN derived soil hydraulic parameters with the simulated soil moisture using the topography based scaling are reported in Table 5. It is seen that the MCMC method provides the least correlation, while the BNN technique has a very high correlation with the topography based technique.

[33] Figure 6 shows the correlations of the simulated soil moistures for each pixel with the corresponding ESTAR soil moisture data product. The correlation values are also reported in Table 11. It is again noticed that the topography-based and BNN-based soil moisture correspond very well with the ESTAR measurements, followed by the homogenization product. The MCMC based soil moisture is

the least correlated overall, with the highest correlation being 0.64 (pixel 9). This observation is in line with correlation values reported by *Das et al.* [2008]. In their study, correlation values between the simulated and AMSR-E soil moistures for the Oklahoma Little Washita region ranged between 0.32 and 0.61, with an average correlation of 0.51 during the summer period, similar in conditions to our study. The low correlation was attributed by *Das et al.* [2008] to the inability of the remote sensor to accurately compensate for the high level of vegetation water during this period. As a result, the AMSR-E values were generally lower during the wetter days.

[34] The ESTAR measurements are made using L-band frequencies of the microwave spectrum, and are hence slightly better equipped to account for the vegetation water content [*Njoku et al.*, 2003]. However, the algorithm developed by *Das et al.* [2008] made use of the long time series of information available for the AMSR-E soil moisture
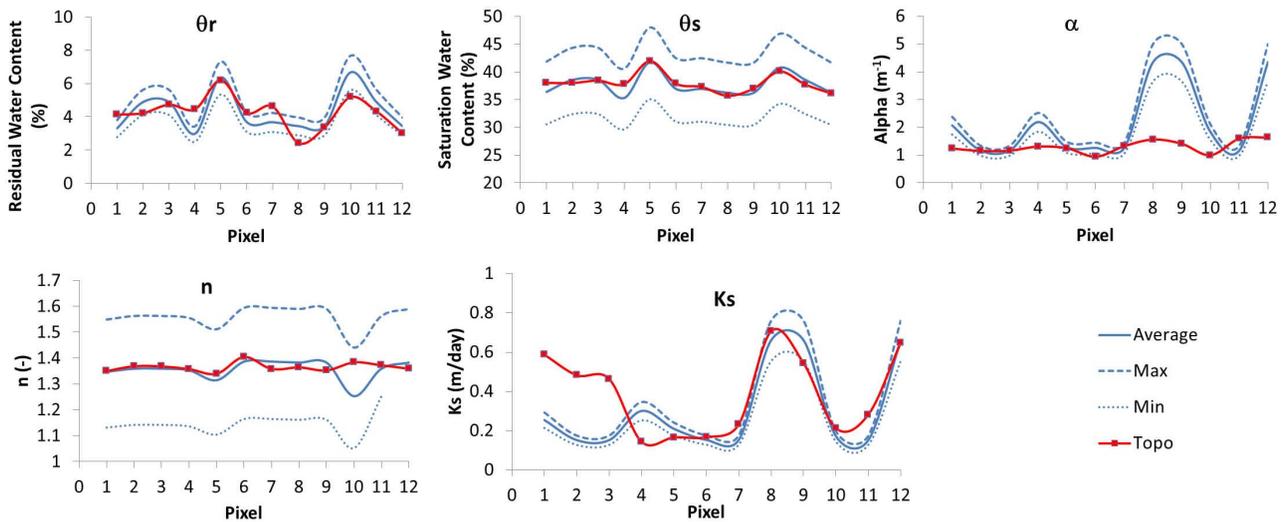
Figure 4. Plots of upscaled soil hydraulic parameters obtained by BNN-based and topography-based upscaling techniques.
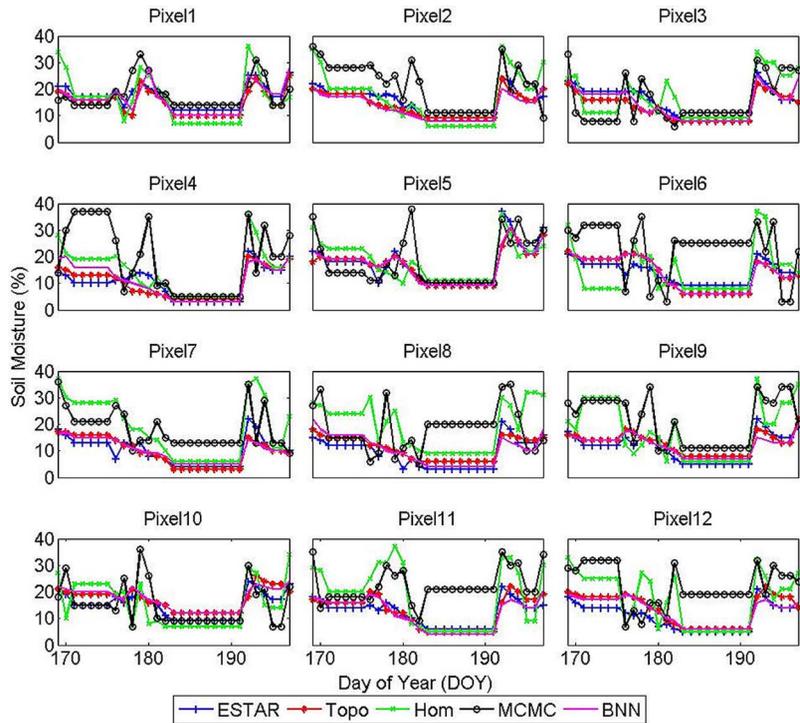
Figure 5. ESTAR measured, and simulated soil moisture signatures for 12 selected pixels. Topo: topography-based scaling; Hom: homogenization; MCMC: Markov chain Monte Carlo-based scaling; BNN: Bayesian neural networks-based scaling.

product. In our study we were restricted to the 16 days of the ESTAR observations. This too could be a factor in the performance of the MCMC algorithm as the time available for the algorithm to settle may not be sufficient.

[35] The higher performance of the BNN scaling algorithm may be attributed to the fact that upscaling generally involves interpolation of soil hydraulic parameter values at the fine scale. Downscaling, on the other hand, could involve extrapolation from the averaged values at the coarse scale. Artificial neural networks work much better with interpolation than with extrapolation. As a result, the

Table 5. Pearson's Correlations of Average Daily Simulated Soil Moisture States From Three Upscaling Methods With Simulated Soil Moisture From Topography-Based Upscaling Scheme[a]

	MCMC	Hom.	BNN
Pixel 1	0.49	0.66[b]	0.81[c]
Pixel 2	0.39	0.95[c]	0.96[c]
Pixel 3	0.66[b]	0.71[c]	0.90[c]
Pixel 4	0.48	0.87[c]	0.95[c]
Pixel 5	0.51[b]	0.58[b]	0.98[c]
Pixel 6	0.24	0.38	1.00[b]
Pixel 7	0.66[b]	0.86[c]	0.98[c]
Pixel 8	0.54[b]	0.79[c]	0.90[c]
Pixel 9	0.31	0.47	0.95[c]
Pixel 10	0.05	0.4	0.88[c]
Pixel 11	0.44	0.61[b]	0.93[c]
Pixel 12	0.14	0.39	0.92[c]

[a]Hom: homogenization; MCMC: Markov Chain Monte Carlo based; BNN: Bayesian neural networks based.
[b]Correlations significant at the 0.05 level.
[c]Correlations significant at the 0.01 level.

soil hydraulic parameters output from the BNN methodology match those from the topography-based scaling technique. It should also be noted that the BNN training inputs included the elevation details, thus making this techniques the closest to the topography-based algorithm.

3.3. Correlation of Average Soil Moisture Based on the Location and Elevation

[36] Based on the precipitation maps for 1997, it was observed that the western portion of the watershed received more rainfall as compared to the eastern parts. This observation is different from that made by *Illston and Basara* [2003], who analyzed the drought conditions in Oklahoma between 1998 and 2000, and note that the western portion of the state is more drought prone as compared to the east. Table 6 shows the correlation coefficients between the simulated and ESTAR measured soil moisture. It is also to be noted that three of the four pixels with the lowest elevations (3, 6, and 7) are situated in the eastern part of the watershed, along with pixel 12. Pixels 1, 4, 5, and 10, having the highest elevations, are located in the western portion of the LW watershed, while the remaining four pixels (8, 9, 11, and 2) are in the middle portion. It may be observed from the ESTAR soil moisture data (Figure 5) that none of the pixels in the middle portion had a significant number of wet days with a soil moisture value above 20%, while two of the three pixels with significant number of dry days, with a soil moisture value less than 10%, were in this region. The fact that the western portion received more rainfall than the east is also verified by most number of pixels with significant number of wet days being in this portion. Pixel 5, which exhibits the most number of wet days, is the western-most pixel

Figure 6. Correlations of average daily simulated soil moisture values with ESTAR measurements. Topo: topography-based scaling; Hom: homogenization; MCMC: Markov chain Monte Carlo-based scaling; BNN: Bayesian neural networks-based scaling.

selected for analysis. Downstream pixels 2 and 3, which also exhibit higher soil moisture states, are located close to the streambed. This would mean that the influx of water into these pixels is significantly more than the others, which is reflected in the higher soil moisture values.

[37] While there is no apparent trend in the soil moisture predictions using the topography-based, MCMC-based, or BNN-based upscaled soil hydraulic parameters, the homogenized parameters performed slightly better at the lower, eastern locations. The worst performance of the homogenized parameters was in the middle portion of the watershed.

3.4. Correlation of Average Soil Moisture State With the Topographic Index

[38] Compound topographic indices $(\ln \frac{A}{\tan(B)})$ [*Beven et al.*, 1984; *Kirkby*, 1975] were computed for each of the 12 pixels suing the fine scale (30 m) elevation data. In the above formulation, *A* is the upslope contributing area at the location of interest, while *B* is the slope of the domain at the location. It has been reported by *Pradhan et al.* [2006] that the grid resolutions of the DEMs used to compute the topographic index have a significant influence on the reliability of the CTI values. As coarser grids are used, the reliability reduces. This is attributed to the fact that the higher resolution topographic characteristics are smoothed out and lost when coarse resolution DEMs are used. Hence we use the fine scale DEM to compute the CTI. The "*dinf*" algorithm suggested by *Tarboton* [1997] was used to compute the flow direction, and thus the upslope contributing area for the compound topographic index (CTI). This algorithm has been shown to provide more realistic representations since the flow directions are not fixed, and flow can occur in multiple directions.

[39] The average CTI values within each of the 12 analysis pixels were computed. The average and variance of the CTI at each pixel are plotted in Figure 7. It can be seen that while there is only a small variation in the average CTI

value, the distribution within each pixel, represented by the error bars, varies more significantly. This signifies that while at the coarse resolution, all the pixels may seem similar with respect to the CTI, at the finer resolution, there are big differences. It is seen that most of the pixels with significant number of wet days (Figure 5) have lesser variation in the CTI. Table 6 shows the correlation coefficients between the simulated and ESTAR soil moisture values. Again, as in the previous section, it is seen that only the homogenized parameters' performance has some relationship with the CTI. The homogenization algorithm performed best in the four pixels which have the highest CTI, while they perform the worst in the four pixels with the lowest CTI. A high CTI value denotes either low changes in the relative elevations within the pixel, or monotonic changes in elevation. A low CTI value, on the other hand, signifies that a more complex terrain exists in the pixel. It can be seen that the three pixels (2, 6, and 7) in which the homogenized parameters performed best, as described in the previous section, have CTI values in the higher range. These pixels all had significant plateau areas with some portion of the domain sloping monotonically toward the flat land. At the other end of the CTI spectrum, pixel 3, although in the eastern third of the watershed, displayed the poorest performance by the homogenized parameters. This pixel had multiple valleys and ridges, thus creating a more complex topographic configuration.

3.5. Correlation of Average Soil Moisture Based on the Land Cover

[40] When the correlation coefficients between the ESTAR observed and simulated soil moistures, are sorted on the basis of the land cover within the pixel (Table 6), it is seen that the pasture pixels have the best overall correlations, followed by the bare pixels for the topography-based and BNN based schemes. The pixels with a winter wheat cover show the least correlation between the simulated and

Table 6. Pearson's Correlations of Average Daily Simulated Soil Moisture States With ESTAR Measurements Across All Days of Observation[a]

	Correlations w.r.t. ESTAR				Average Elevation (m)	Location	Average CTI	Land Cover
	Topo.	Hom.	MCMC	BNN				
Pixel 1	0.87[b]	0.75[b]	0.58[c]	0.77[b]	446	West	7.332	Wheat
Pixel 2	0.88[b]	0.87[b]	0.55[c]	0.84[b]	355	Mid	7.312	Pasture
Pixel 3	0.88[b]	0.62[c]	0.57[c]	0.81[b]	369	East	6.656	Pasture
Pixel 4	0.82[b]	0.74[b]	0.49	0.77[b]	408	West	6.846	Pasture
Pixel 5	0.89[b]	0.76[b]	0.60[c]	0.90[b]	410	West	6.846	Bare
Pixel 6	0.76[b]	0.73[b]	0.45	0.76[b]	345	East	7.379	Pasture
Pixel 7	0.75[b]	0.82[b]	0.52[c]	0.72[b]	341	East	7.396	Pasture
Pixel 8	0.88[b]	0.84[b]	0.60[c]	0.74[b]	407	Mid	7.128	Bare
Pixel 9	0.84[b]	0.63[c]	0.64[c]	0.73[b]	392	Mid	6.709	Pasture
Pixel 10	0.67[c]	0.75[b]	0.53[c]	0.84[b]	419	West	7.274	Wheat
Pixel 11	0.76[b]	0.71[b]	0.61[c]	0.76[b]	377	Mid	7.085	Wheat
Pixel 12	0.84[b]	0.67[c]	0.44	0.76[b]	394	East	7.247	Bare

[a]Hom: homogenization; MCMC: Markov Chain Monte Carlo based; BNN: Bayesian neural networks based.
[b]Correlations significant at the 0.01 level.
[c]Correlations significant at the 0.05 level.

ESTAR measure soil moistures. This could be due to crop management practices such as harvesting, or water logging taking place during this period, which has not been accounted for in our study. Furthermore, it is seen that most of the pixels with significant wet days have a pasture cover. The pixel with most wet days (pixel 5) has a bare soil cover. The homogenization and MCMC methods had no apparent pattern associated with the land cover.

3.6. Comparison of Generated Surface Runoff

[41] Streamflow gauges at two locations (Figure 1) were used to compare the generated surface runoff quantities using the upscaled soil hydraulic parameters from the four scaling algorithms. The upstream gauge (USGS designation SG442) is situated near pixel 5, while the downstream gauge (SG447) is near pixel 9. Surface fluxes routed to the pixels containing the stream gauges are compared with the daily stream discharge data from these gauges as shown in Figures 8 and 9. While the four scaling methods resulted in different values of the stream flux, the general trend is similar in all cases. It is seen that the plot for the upstream

Figure 7. Average compound topographic index of 12 selected pixels derived from 30 m resolution DEM. Error bars represent variance of CTI within each pixel.

gauge (Figure 8) displays high degrees of correlation between the measured and modeled fluxes. This is due to the small contributing area for this gauge. It must also be noted that the correlations are reported after correcting for a 1 day lag in the modeled fluxes. This lag is attributed to the time scale (daily) at which the flow routing is implemented between pixel domains in the watershed.

[42] At the downstream gauge (Figure 9), it is seen that the two scaling methods which take the topography into consideration have higher correlations between the measured and modeled fluxes. With a larger contributing area, the flux discharge at this gauge is more dependent on the topography than the upstream gauge. In this case, the correlations have been corrected for a 2 day lag. It is expected that there would be a threshold value for the catchment size beyond which the lag time would not rise. At this threshold size the travel time for surface runoff from the nearer pixels to the stream would dominate those from the farther pixels, thus creating a spread out response.

[43] Computational restraints permitting, if the entire watershed were to be simulated in HYDRUS as a single domain, slightly improved matches are expected between the simulated and measured streamflows. This would be attributed mainly to the fact that an offline routing algorithm would not be necessary for the overland and subsurface fluxes. This could result in elimination of the response time lag, and also a more continuous real-time distribution of soil moisture and fluxes.

[44] The objective of this study was to compare the performances of the four upscaling algorithms under similar conditions. From the results obtained, it was seen that, overall, the two algorithms (topography-based and BNN-based) which accounted for topographic variations in some form performed better than the two algorithms (homogenization, and MCMC-based) that did not factor in the effect of the topography. It has been previously hypothesized [*Jana and Mohanty*, 2012a] that different physical controls dominate soil property and moisture variability at different scales. It is thought that the soil texture and structure dominate at the smaller scales, while topography exerts more influence at hillslope (kilometer) scales. Beyond that, at regional scales, the vegetation or land cover may be the
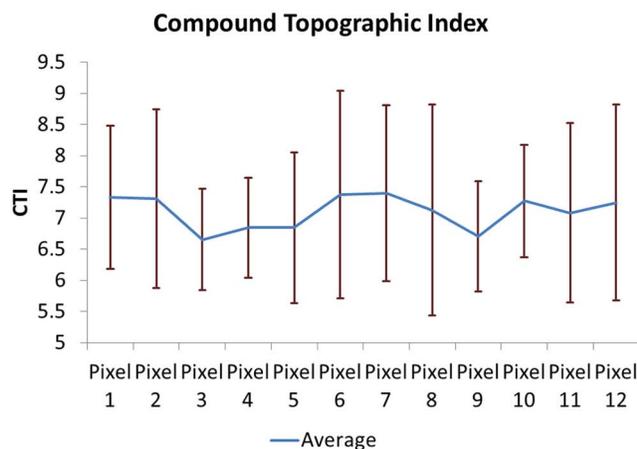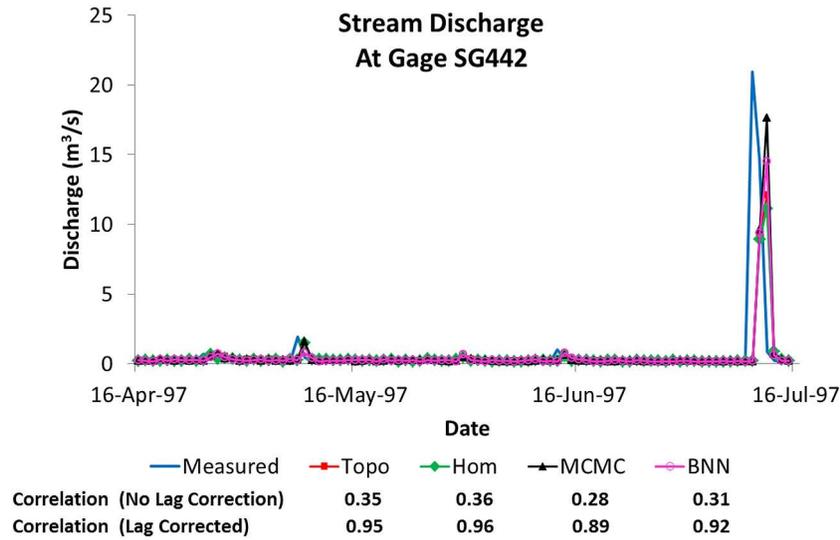
Figure 8. Comparison of stream discharge at upstream gauge. Correlations are provided between measured and simulated values, with and without correction for lag in model response time. Topo: topography-based scaling; Hom: homogenization; MCMC: Markov chain Monte Carlo-based scaling; BNN: Bayesian neural networks-based scaling.

dominant control, giving way to the climate at continental scales. The above discussion brings out the fact that the homogenized parameters fared poorly in pixels with complex topographic configurations. However, the topography-based scaling algorithm, and the BNN-based technique, which incorporate the elevation differences in their routines fared equally well across all scenarios. The findings of this study strengthen the argument that at hillslope scales, the topography is a dominant factor in dictating the soil hydraulic parameter values, and thus the soil water dynamics.

The differences in the correlations based on the land cover suggest that the vegetation is exerting some influence on the soil moisture variation at the hillslope scale too.

[45] From this study it can be inferred that when the domain of interest and the support dimension are small, the choice of the upscaling algorithm does not make much difference since the soil parameter variability is dictated mainly by the soil texture and structure. However, at hillslope scales, selection of upscaling algorithms that account for the effect of the changing topography at that scale
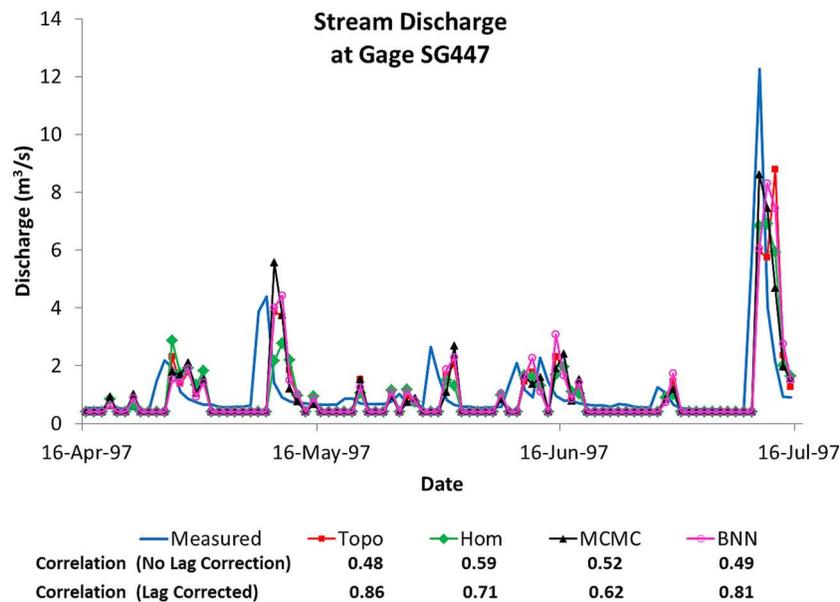
Figure 9. Comparison of stream discharge at downstream gauge. Correlations are provided between measured and simulated values, with and without correction for lag in model response time. Topo: topography-based scaling; Hom: homogenization; MCMC: Markov chain Monte Carlo-based scaling; BNN: Bayesian neural networks-based scaling.

significantly improves the effective values for the soil hydraulic parameters. The two methods tested here which account for topography are designed such that when the domain has a lower topographic complexity, the effect of the topography is reduced. Hence, they can be assumed to be more generic scaling algorithms as compared to the two that do not include topography.

[46] Based on the simulated streamflow, users interested in flood analysis may prefer the MCMC-based method over the others since this method resulted in consistently higher estimates of the stream discharge during the peaks. Similarly, one interested in drought planning may prefer the topography-based scaling technique due to its better match with the observed low flow conditions.

[47] While the upscaling methodologies have been tested at only one watershed in this study, the original articles in which the methods have been developed report their performances under different hydroclimatic conditions. For example, the topography-based scaling algorithm has been tested by *Jana and Mohanty* [2012a, 2012b] at the Little Washita watershed as well as the Walnut Creek watershed in Iowa, apart from a synthetic study under different topographic scenarios. Similarly, *Das et al.* [2008] have tested the MCMC-based algorithm at the Little Washita (OK), Walnut Creek (IA), and the Walnut Gulch (AZ) watersheds. The BNN-based scaling algorithm has been applied at different locations in the Rio Grande basin and in the Walnut Creek watershed by *Jana et al.* [2008] and *Jana and Mohanty* [2011]. As such, the algorithms have been shown to be applicable to upscaling of soil hydraulic parameters under different conditions of climate, vegetation, topography, and soils. While the numerical value of the scale parameters in the change from site to site, the methodologies themselves hold good for all sites.

[48] Certain assumptions were made in setting up the hydrologic model such as the depths to the water table, the depths of the root zone, and the initial condition of the soil moisture. While it is always desirable to have the most accurate information when modeling, such assumptions are sometimes necessary as a trade-off between accuracy and practicality. If the water table data were much different from the model assumptions, different volumes of subsurface fluxes, soil water storage, and consequently surface runoff would be seen. Changes in the rooting depth would affect the ET fluxes, and also the soil moisture in the top layers. However, from the hydrologic simulations, we see that the simulated fluxes and soil moisture values match the variability in the observed values. Hence, the assigned water tables and rooting depths can be assumed to be reasonably close to reality. The initial conditions would definitely dictate the domain responses in the early phases of the simulations. However, after a certain duration, the initial conditions hold no influence on the simulations. This is the reason why we designate the first two months of the simulation as the model spin-up time and discard them from the analysis.

[49] It is possible that different soil parameters may be better upscaled by different methodologies. In such a scenario, the best set of effective upscaled parameters would be obtained by using a suite of algorithms instead of a single method. However, our aim was to obtain the overall best set of effective parameters at the coarse resolution, and to find out which single one of the four upscaling method-

ologies compared here resulted in the best match to observed data. Hence we do not consider the performance of individual parameters. Nevertheless, this is a suitable subject for further investigation.

4. Conclusions

[50] Four different techniques of upscaling soil hydraulic parameters from the 30 m resolution to a 1 km resolution were compared at the Little Washita watershed. A topography-based aggregation scheme, a simple homogenization method, an MCMC-based stochastic technique, and a Bayesian neural network approach to the upscaling problem were analyzed in this study. The equivalence of the upscaled parameters was tested by simulating water flow for the watershed pixels in HYDRUS-3-D, and comparing the resultant soil moisture states with data from ESTAR airborne sensor during the SGP97 hydrology experiment.

[51] Correlations of simulated and observed soil moistures were compared across time, location, elevation, vegetative cover, and with respect to topographic indices, with varying results. It was inferred that the inclusion of topography in the hydraulic parameter scaling algorithm accounts for much of the variability. The topography-based scaling algorithm, followed by the BNN technique, were able to capture much of the variation in soil hydraulic parameters required to generate equivalent soil moisture states in a coarsened domain. The homogenization and MCMC methods, which did not account for topographic variations performed poorly in providing effective soil hydraulic parameters at the coarse scale.

References

Allen, P. B., and J. W. Naney (1991), Hydrology of Little Washita River Watershed: Oklahoma—Data and analyses, *ARS-90*, 74 pp, U.S. Dep. of Agric., U.S. Gov. Print. Off., Washington, D.C.

Beven, K. J., M. J. Kirkby, N. Schofield, and A. F. Tagg (1984), Testing a physically-based flood forecasting-model (Topmodel) for three UK catchments, *J. Hydrol.*, *69*(1), 119–143.

Elliott, R., F. Schiebe, K. Crawford, K. Peter, and W. Puckett (1993), A unique data capability for natural resources studies, paper no. 93-2529, presented at Int. Winter Meeting, Am. Soc. Agr. Eng., Chicago, Ill., Dec. 14–17, 1993.

Das, N. N., B. P. Mohanty, and E. G. Njoku (2008), A Markov chain Monte Carlo algorithm for upscaled soil-vegetation-atmosphere-transfer modeling to evaluate satellite-based soil moisture measurements, *Water Resour. Res.*, *44*(5), W05416, doi:10.1029/2007WR006472.

Gelman, A., J. B. Carlin, H. S. Stern, and D. B. Rubin (1995), *Bayesian Data Analysis*, CRC, Boca Raton, FL.

Illston, B. G., and J. B. Basara (2003), Analysis of short term droughts in Oklahoma, *EOS, Trans.*, *84*(17), 157–161.

Iorgulescu, I., and A. Musy (1997), Generalization of TOPMODEL for a power law transmissivity profile, *Hydrol. Process.*, *11*, 1353–1355.

Jackson, T. J., D. M. LeVine, A. Y. Hsu, A. Oldak, P. J. Starks, and C. T. Swift (1999), Soil moisture mapping at regional scales using microwave radiometry: The Southern Great Plains hydrology experiment, *IEEE Trans. Geosci. Remote Sens.*, *37*, 2136–2151.

Jana, R. B., and B. P. Mohanty (2011), Enhancing PTFs with remotely sensed data for fine scale soil water retention estimation, *J. Hydrol.*, *399*, 201–211.

Jana, R. B., and B. P. Mohanty (2012a), On topographic controls of soil hydraulic parameter scaling at hillslope scales, *Water Resour. Res.*, doi:10.1029/2011WR011204, in press.

Jana, R. B., and B. P. Mohanty (2012b), A topography-based scaling algorithm for soil hydraulic parameters at hill-slope scales: Field testing, *Water Resour. Res.*, doi:10.1029/2011WR011205, in press.

Jana, R. B., B. P. Mohanty, and E. P. Springer (2008), Multiscale Bayesian neural networks for soil water content estimation, *Water Resour. Res.*, *44*(8), W08408, doi:10.1029/2008WR006879.

Kirkby, M. J. (1975), Hydrograph modeling strategies, in *Process in Physical and Human Geography*, edited by R. Peel, M. Chisholm, and P. Haggett, pp. 69–90, Heinemann, London.

Kollet, S. J., and R. M. Maxwell (2008), Capturing the influence of groundwater dynamics on land surface processes using an integrated, distributed watershed model, *Water Resour. Res.*, *44*, W02402, doi:10.1029/2007WR006004.

Miller, E. E., and R. D. Miller (1956), Physical theory for capillary flow phenomena, *J. Appl. Phys.*, *27*(4), 324–332.

Mohanty, B. P., and Z. Mousli (2000), Saturated hydraulic conductivity and soil water retention properties across a soil-slope transition, *Water Resour. Res.*, *36*(11), 3311–3324, doi:10.1029/2000WR900216.

Mohanty, B. P., P. J. Shouse, D. A. Miller, and M. T. van Genuchten (2002), Soil property database: Southern Great Plains 1997 Hydrology Experiment, *Water Resour. Res.*, *38*(5), 1047, doi:10.1029/2000 WR000076.

Njoku, E. G., T. J. Jackson, V. Lakshmi, T. K. Chan, and S. V. Nghiem (2003), Soil moisture retrieval from AMSR-E, *IEEE Trans. Geosci. Remote Sensing*, *41*(2), 215–229.

Pradhan, N. R., Y. Tachikawa, and K. Takara (2006), A downscaling method of topographic index distribution for matching the scales of model application and parameter identification, *Hydrol. Process.*, *20*(6), 1385–1405, doi:10.1002/Hyp.6098.

Schaap, M. G., F. J. Leij, and M. T. V. Genuchten (2001), Rosetta: A computer program for estimating soil hydraulic parameters with hierarchical pedotransfer functions, *J. Hydrol.*, *251*(3–4), 163–176.

Shouse, P. J., and B. P. Mohanty (1998), Scaling of near-saturated hydraulic conductivity measured using disc infiltrometers, *Water Resour. Res.*, *34*(5), 1195–1205, doi:10.1029/98WR00318.

Šimůnek, J., M. T. V. Genuchten, and M. Šejna (2006), The HYDRUS software package for simulating two- and three-dimensional movement of water, heat, and multiple solutes in variably-saturated media: Technical manual, Version 1.0, PC-Progress, Prague, Czech Republic.

Tarboton, D. G. (1997), A new method for the determination of flow directions and contributing areas in grid digital elevation models, *Water Resour. Res.*, *33*(2), 309–319.

van Genuchten, M. T. (1980), A closed-form equation for predicting the hydraulic conductivity of unsaturated soils, *Soil Sci. Soc. Am. J.*, *44*, 892–898.

Vereecken, H., R. Kasteel, J. Vanderborght, and T. Harter (2007), Upscaling hydraulic properties and soil water flow processes in heterogeneous soils: A review, *Vadose Zone J*, *6*, 1–28.

Wu, J., and H. Li (2006), Concepts of scale and scaling, in *Scaling and Uncertainty Analysis in Ecology: Methods and Applications*, edited by J. Wu, K. B. Jones, and H. Li, pp. 3–15, Springer, Dordrecht, Netherlands.

Yager, R. R. (1996), On mean type aggregation, *IEEE Trans. Syst. Man Cybern. Pt. B Cybern.*, *26*(2), 209–221.

Yager, R. R. (2001), The power average operator, *IEEE Trans. Syst. Man Cybern. Pt. A Syst. Hum.*, *31*(6), 724–731.

Zhu, J., and B. P. Mohanty (2002), Spatial averaging of van Genuchten hydraulic parameters for steady-state flow in heterogeneous soils: A numerical study, *Vadose Zone J*, *1*(2), 261–272.

R. B. Jana and B. P. Mohanty, Department of Biological and Agricultural Engineering, MS 2117, Texas A&M University, College Station, TX 77843, USA. (bmohanty@tamu.edu)